XVI International Conference on Computational Plasticity. Fundamentals and Applications
COMPLAS 2021
E. Oñate, D. Peric, M. Chiumenti and Eduardo de Souza Neto (Eds)

NUMERICAL INVESTIGATION OF LOAD SEQUENCE EFFECT AND ENERGY DISSIPATION IN CONCRETE DUE TO COMPRESSIVE FATIGUE LOADING USING THE NEW MICROPLANE FATIGUE MODEL MS1

M. AGUILAR*, A. BAKTHEER* AND R. CHUDOBA*

* Institute of Structural Concrete
RWTH Aachen University
Mies-van-der-Rohe-Straße 1 , 52074 Aachen , Germany
e-mail: maguilar@imb.rwth-aachen.de, web page: http://www.imb.rwth-aachen.de/

Key words: Concrete, Fatigue, Cyclic loading, Energy dissipation, Loading sequence effect, Variable amplitudes, Damage

Abstract. Modeling the fatigue behavior of concrete is a challenging task that has attracted the interest of researchers during the last decades. A new formulation of a microplane fatigue model denoted as MS1 introduced by the authors is employed. It aims to capture the basic inelastic mechanisms that are driving the tri-axial stress redistribution within a material zone during the fatigue damage process in concrete. In order to do so, the fatigue damage evolution is linked to a measure of the cumulative inelastic shear strain, reflecting the accumulation of fatigue damage owing to internal shear/sliding between aggregates at subcritical load levels.

In the first place, numerical studies are presented, in which the elementary interface behavior and dissipation mechanisms are evaluated. Later on, an evaluation of the energy dissipation of experimental tests in terms of their hysteretic loops is displayed. This approach is called into question as available experimental data strongly suggests that this method underestimates the actual amount of energy being dissipated. The microplane material model MS1, which is able to reproduce the concrete behavior under monotonic, cyclic, and fatigue loading with consistent sets of material parameters, has been employed for evaluating the contributions of the different dissipative mechanisms for different loading scenarios. Further studies assessing the ability of the model to reproduce the sequence effect for fatigue loading with varying amplitudes in terms of an energetic-based approach are presented.

1 INTRODUCTION

Concrete fatigue damage behavior, i.e. progressive degradation of the material properties and accumulation of inelastic strains induced by subcritical cyclic loading, is a phenomenon that has not been sufficiently understood. Understanding it is crucial since an increasing amount of slender concrete structures are being constructed in which fatigue effects play a considerable role. Although many efforts have been made towards better understanding this phenomenon, the actual verification methods that are being

used for considering it in design are simple and rough, and they sometimes contradict the experimental evidence.

Standard procedures for performing a fatigue verification in cases where variable actions produce fatigue effects, consist of assuring that the stress values developed by the concrete for the given loading are within a stipulated range [1]. Another strategy would be to study the fatigue life of some critical structural components, assuring that they do not fail during their service life [2]. This is usually done by considering loading scenarios with constant amplitudes which have been studied in more detail. Verification procedures for fatigue loading with varying amplitudes and sequences consist of the application of the well-known Palmgren-Miner (P-M) rule, which has been put in question due to its lack of agreement with experimental results [3].

The authors aim to shed some light on the basic mechanisms that are driving the fatigue damage behavior in concrete. One of the main goals of the authors is to establish a link between the energy being dissipated during the fatigue damage process and the number of cycles that the material can resist. This would allow making correct predictions of its behavior under any kind of circumstances, by making use of simplified methods based on adequate energetic assessments, rather than trying to evaluate it on a basis of empirical equations which is limited for specific cases.

2 MICROPLANE MATERIAL MODEL MS1

With this intention, the authors have recently introduced the microplane material model MS1 [4]. The key idea of this material model is to link the fatigue damage evolution to a measure of the cumulative inelastic shear strain. This hypothesis is grounded on experimental observations presented by Skarzynski et al. [5], where crack nucleation and propagation during fatigue loading occurred along with the interfaces between the cement paste and the aggregates, as depicted in Fig 1a. Thermodynamically based constitutive laws governing the macroscopic behavior are defined at the microplane level. The present model is developed within the context of the microplane theory using a homogenization scheme based on the principle of energy equivalence with a direct tensorial representation of the effective elastic stiffness.

Thermodynamically based constitutive laws governing the macroscopic behaviour are defined on the generic microplanes. The macroscopic thermodynamic potential is expressed as the sum of the normal and tangential Helmholtz free energies:

$$\psi^{\mathrm{mac}} = \frac{3}{2\pi}\int_{\Omega}\psi^{\mathrm{mic}}d\Omega = \frac{3}{2\pi}\int_{\Omega}\psi_{\mathrm{N}}d\Omega + \frac{3}{2\pi}\int_{\Omega}\psi_{\mathrm{T}}d\Omega. \tag{1}$$

The projection of the thermodynamic potentials onto the normal and tangential direction allows introducing distinguished dissipative mechanisms for each direction, which are summarized in Fig. 1b.

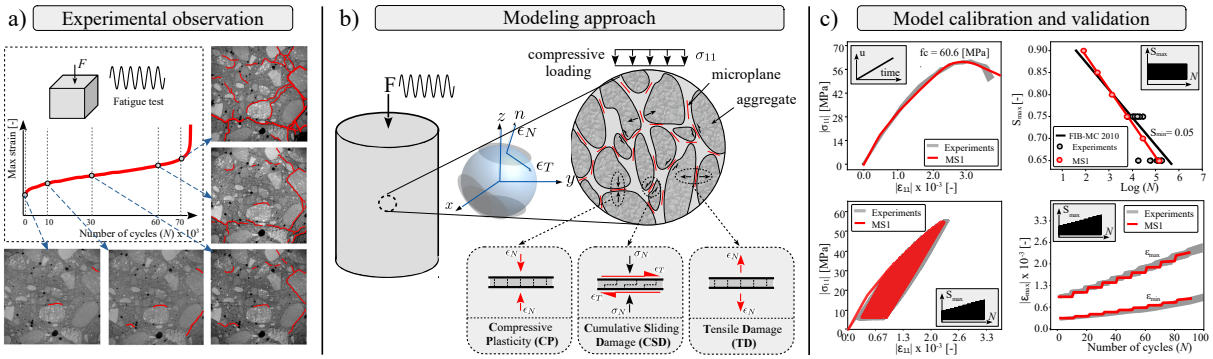

Figure 1: Summary of MS1 model: a) Experimental observations of the microcrack development under fatigue loading using X-ray micro-CT images presented by Skarzynski et al. [5], b) Dissipative mechanisms included in the proposed microplane model MS1 and illustration of the microstructure containing a system of dissipative microplanes that are integrated within a 3D hemisphere idealization, c) material model calibration and validation for monotonic, cyclic and fatigue behavior.

Normal direction: The normal direction microplane thermodynamic potential takes the form

$$\rho\psi_{\mathrm{N}} = \frac{1}{2}\left[1 - H(\sigma_{\mathrm{N}})\omega_{\mathrm{N}}\right] E_{\mathrm{N}}(\varepsilon_{\mathrm{N}} - \varepsilon_{\mathrm{N}}^{\mathrm{p}})^2 + \frac{1}{2}K_{\mathrm{N}} z_{\mathrm{N}}^2 + \frac{1}{2}\gamma_{\mathrm{N}}\alpha_{\mathrm{N}}^2 + f(r_{\mathrm{N}}), \tag{2}$$

where $\psi_{\mathrm{N}}^{\mathrm{mic}}$ represents the Helmholtz free energy of the normal direction, ρ the material density and E_{N} is the normal elastic stiffness, being

$$E_{\mathrm{N}} = \frac{E}{(1-2\nu)}, \tag{3}$$

where E is the Young's modulus and ν is the Poisson's ratio. $H(\sigma_{\mathrm{N}})$ is a Heaviside function for switching the normal behaviour between tension and compression. If the microplane is subjected to tension, then $H(\sigma_{\mathrm{N}}^{+}) = 1$, and damage internal variables may evolve, while plastic ones remain unchanged. If the microplane is subjected to compression, then $H(\sigma_{\mathrm{N}}^{-}) = 0$, plastic phenomena may take place, while normal damage evolution does not occur. K_{N} and γ_{N} are the isotropic and kinematic hardening moduli, respectively.

The thermodynamic internal variables are: the plastic normal strain $\varepsilon_{\mathrm{N}}^{\mathrm{p}}$, damage variable ω_{N} going from 0 to 1, isotropic hardening z_{N} and kinematic hardening α_{N} variables. The function $f(r_{\mathrm{N}})$ defines a consolidation function associated with the damage.

The thermodynamic forces are obtained by differentiating the thermodynamic potential (2) with respect to each internal variable.

Tangential direction: Tangential cumulative damage is considered as the primal source of fatigue damage. This mechanism drives the material deterioration at subcritical loading levels. For describing the tangential behavior of a microplane, the pressure sensitive interface model with fatigue damage driven by cumulative inelastic slip presented in [6] is adopted. Therefore, the tangential direction microplane thermodynamic potential reads

$$\rho\psi_{\mathrm{T}} = \frac{1}{2}(1-\omega_{\mathrm{T}})E_{\mathrm{T}}(\boldsymbol{\varepsilon}_{\mathbf{T}} - \boldsymbol{\varepsilon}^{\boldsymbol{\pi}}_{\mathbf{T}}) \cdot (\boldsymbol{\varepsilon}_{\mathbf{T}} - \boldsymbol{\varepsilon}^{\boldsymbol{\pi}}_{\mathbf{T}}) + \frac{1}{2}K_{\mathrm{T}} z_{\mathrm{T}}^2 + \frac{1}{2}\gamma_{\mathrm{T}}\boldsymbol{\alpha}_{\mathbf{T}} \cdot \boldsymbol{\alpha}_{\mathbf{T}}, \tag{4}$$

where $\psi_{\mathrm{T}}^{\mathrm{mic}}$ is the Helmholtz free energy of the tangential direction, ρ the material density and E_{T} is the tangential elastic stiffness, being

$$E_{\mathrm{T}} = \frac{E(1-4\nu)}{(1+\nu)(1-2\nu)}, \tag{5}$$

where E is the Young's modulus and ν is the Poisson's ratio. K_{T} and γ_{T} are the isotropic and kinematic hardening moduli, respectively. The thermodynamic internal variables are the inelastic tangential strain vector, i.e. the sliding strain vector defining the irreversible strain $\boldsymbol{\varepsilon}^{\boldsymbol{\pi}}_{\mathbf{T}}$, the damage variable ω_{T} ranging from 0 to 1, the internal variables of isotropic hardening z_{T} and kinematic hardening vector $\boldsymbol{\alpha}_{\mathbf{T}}$. The corresponding thermodynamic forces are derived by differentiating the thermodynamic potential (4) with respect to each internal variable.

Further features and capabilities of the microplane material model MS1 are discussed at [4]. This includes aspects such as the ability of the material model to reproduce stress redistribution at the level of the material point and anisotropic damage evolution. A calibration and validation procedure was conducted for monotonic, cyclic, and fatigue behavior for three different types of concretes, based on an accompanying experimental campaign. This is summarized in Fig. 1c.

3 ENERGY DISSIPATION UNDER CYCLIC AND FATIGUE LOADING

3.1 Evaluation method of fatigue-induced energy dissipation

The profile of energy dissipation during the fatigue loading history represents an important characteristic of the material response that has been included in the evaluation of the experimental studies by several authors in the past [7, 8, 9]. In the cited work, the energy dissipation was evaluated as a sum of the areas enclosed by the hysteretic loops. This approach, however, neglects the energy that has been dissipated outside the loops.

To demonstrate the significance of the outside-loop dissipation, let us consider an example depicted in Fig. 2 showing the experimental response obtained in beam-end-test [10]. A step-wise increasing cyclic loading applied as pullout load as indicated in Fig. 2a induced the displacement response shown in Fig. 2b.

The corresponding area of hysteretic loops representing the energy dissipated per cycle is shown in Fig. 2c. Apparently, the area enclosed by the pullout curve outside the hysteretic loops is significantly larger than the area of the hysteretic loops themselves. This is also confirmed by the fact that the energy dissipation plotted in Fig. 2c does not reflect the rapid growth of the inelastic displacement shown in Fig. 2b. This example documents that the evaluation of energy dissipation including only the hysteretic loops is insufficient and leads to its underestimation.

As it is not possible to experimentally evaluate the actual energy dissipated due to cyclic fatigue loading, it is necessary to use a material model describing the dissipative effects as exemplified by the microplane material model MS1 summarized in Sec. 2.

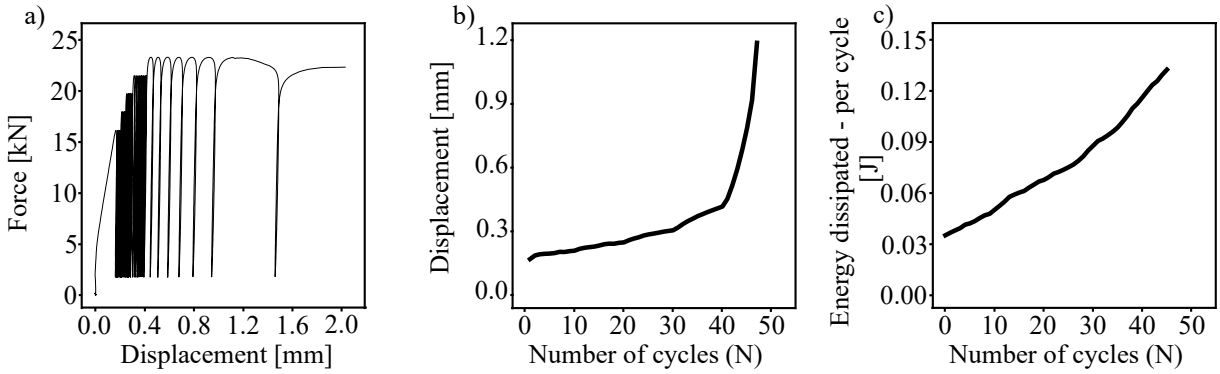

Figure 2: Experimental data, a) stress-strain curve, b) fatigue creep curve, c) dissipated energy per cycle

3.2 Evaluation of the energy dissipation for microplane material model MS1

The energy dissipation of the microplane material model MS1 is evaluated with reference to the Clausius-Duhem inequality stating that

$$\dot{\mathcal{D}}^{\mathrm{N}}_{\mathrm{int}} = -\rho\dot{\psi}_{\mathrm{N}} + \sigma_{\mathrm{N}}\dot{\varepsilon}_{\mathrm{N}} \geq 0, \tag{6}$$

which, after substitution for $\dot{\psi}_{\mathrm{N}}$ and application of the chain rule, reads

$$\dot{\mathcal{D}}^{\mathrm{N}}_{\mathrm{int}} = -\left(\frac{\partial\rho\psi_{\mathrm{N}}}{\partial\varepsilon^{e}_{\mathrm{N}}}\dot{\varepsilon}_{\mathrm{N}} - \frac{\partial\rho\psi_{\mathrm{N}}}{\partial\varepsilon^{p}_{\mathrm{N}}}\dot{\varepsilon}^{p}_{\mathrm{N}} + \frac{\partial\rho\psi_{\mathrm{N}}}{\partial z_{\mathrm{N}}}\dot{z}_{\mathrm{N}} + \frac{\partial\rho\psi_{\mathrm{N}}}{\partial\alpha_{\mathrm{N}}}\dot{\alpha}_{\mathrm{N}} + \frac{\partial\rho\psi_{\mathrm{N}}}{\partial\omega_{\mathrm{N}}}\dot{\omega}_{\mathrm{N}} + \frac{\partial\rho\psi_{\mathrm{N}}}{\partial r_{\mathrm{N}}}\dot{r}_{\mathrm{N}}\right) + \sigma_{\mathrm{N}}\dot{\varepsilon}_{\mathrm{N}}. \tag{7}$$

Realizing that the derivative of the Helmholtz potential with respect to elastic strain represents the stress variable, i.e.

$$\sigma_{\mathrm{N}} = \frac{\partial\psi_{\mathrm{N}}}{\partial\varepsilon^{\mathrm{e}}_{\mathrm{N}}}, \tag{8}$$

the energy dissipation in the normal direction is obtained as by integrating the dissipation rates over the pseudo time variable t used to control the nonmonotonic loading scenarios:

$$\mathcal{D}^{\mathrm{N}}_{\mathrm{int}} = \int_0^t \left[\sigma_{\mathrm{N}}\dot{\varepsilon}^{p}_{\mathrm{N}} - Z_{\mathrm{N}}\dot{z}_{\mathrm{N}} - X_{\mathrm{N}}\dot{\alpha}_{\mathrm{N}} + Y_{\mathrm{N}}\dot{\omega}_{\mathrm{N}} - R_{\mathrm{N}}\dot{r}_{\mathrm{N}}\right] \mathrm{d}t. \tag{9}$$

The dissipation of energy for the tangential direction is evaluated in a similar manner as for the normal direction starting with the Clauius-Duhem inequality, i.e.

$$\dot{\mathcal{D}}^{\mathrm{T}}_{\mathrm{int}} = -\rho\dot{\psi}_{\mathrm{T}} + \boldsymbol{\sigma}_{\mathbf{T}}\dot{\boldsymbol{\varepsilon}}_{\mathbf{T}} \geq 0, \tag{10}$$

rendering the expression for the energy dissipation in terms of the internal variables as

$$\dot{\mathcal{D}}^{\mathrm{T}}_{\mathrm{int}} = -\left(\frac{\partial\rho\psi_{\mathrm{T}}}{\partial\boldsymbol{\varepsilon}^{\mathbf{e}}_{\mathbf{T}}}\dot{\boldsymbol{\varepsilon}}_{\mathbf{T}} - \frac{\partial\rho\psi_{\mathrm{T}}}{\partial\boldsymbol{\varepsilon}^{\boldsymbol{\pi}}_{\mathbf{T}}}\dot{\boldsymbol{\varepsilon}}^{\boldsymbol{\pi}}_{\mathbf{T}} + \frac{\partial\rho\psi_{\mathrm{T}}}{\partial z_{\mathrm{T}}}\dot{z}_{\mathrm{T}} + \frac{\partial\rho\psi_{\mathrm{T}}}{\partial\boldsymbol{\alpha}_{\mathbf{T}}}\dot{\boldsymbol{\alpha}}_{\mathbf{T}} + \frac{\partial\rho\psi_{\mathrm{T}}}{\partial\omega_{\mathrm{T}}}\dot{\omega}_{\mathrm{T}}\right) + \boldsymbol{\sigma}_{\mathbf{T}}\dot{\boldsymbol{\varepsilon}}_{\mathbf{T}}. \tag{11}$$

Due to the fact for the first term represents the tangential stress

$$\boldsymbol{\sigma}_{\mathbf{T}} = \frac{\partial \rho \psi_{\mathrm{T}}}{\partial \boldsymbol{\varepsilon}^{\mathrm{e}}_{\mathbf{T}}}, \tag{12}$$

dissipation for the tangential direction simplifies to

$$\mathcal{D}^{\mathrm{T}}_{\mathrm{int}} = \int_0^t \left[\boldsymbol{\sigma}_{\mathbf{T}} \cdot \dot{\boldsymbol{\varepsilon}}^{\boldsymbol{\pi}}_{\mathbf{T}} - Z_{\mathrm{T}} \dot{z}_{\mathrm{T}} - \boldsymbol{X}_{\mathbf{T}} \cdot \dot{\boldsymbol{\alpha}}_{\mathbf{T}} + Y_{\mathrm{T}} \dot{\omega}_{\mathrm{T}} \right] \mathrm{d}t. \tag{13}$$

Elementary studies of the behavior of a single microplane for the normal and tangential directions are shown in Fig. 3 in order to visualize its qualitative energy dissipation profiles. In the first row, the normal stress-strain curve and energy dissipation due to plasticity and damage is shown for monotonic and cyclic loading. The second row shows the stress and dissipation response for cyclic loading. Fig. 3a documents the ability of the model to capture the unilateral effect, i.e. the transition between the compressive plasticity and tensile damage. While the normal stiffness decreases in the tensile regime, its reduction does not have any effect on the compressive stiffness. Correspondingly, plastic dissipation evolves only under compression (Fig. 3b), and damage dissipation under tension (Fig. 3c). The response to cyclic tangential loading depicted in Fig. 3d exhibits isotropic and kinematic hardening, as well as, a noticeable reduction of the material

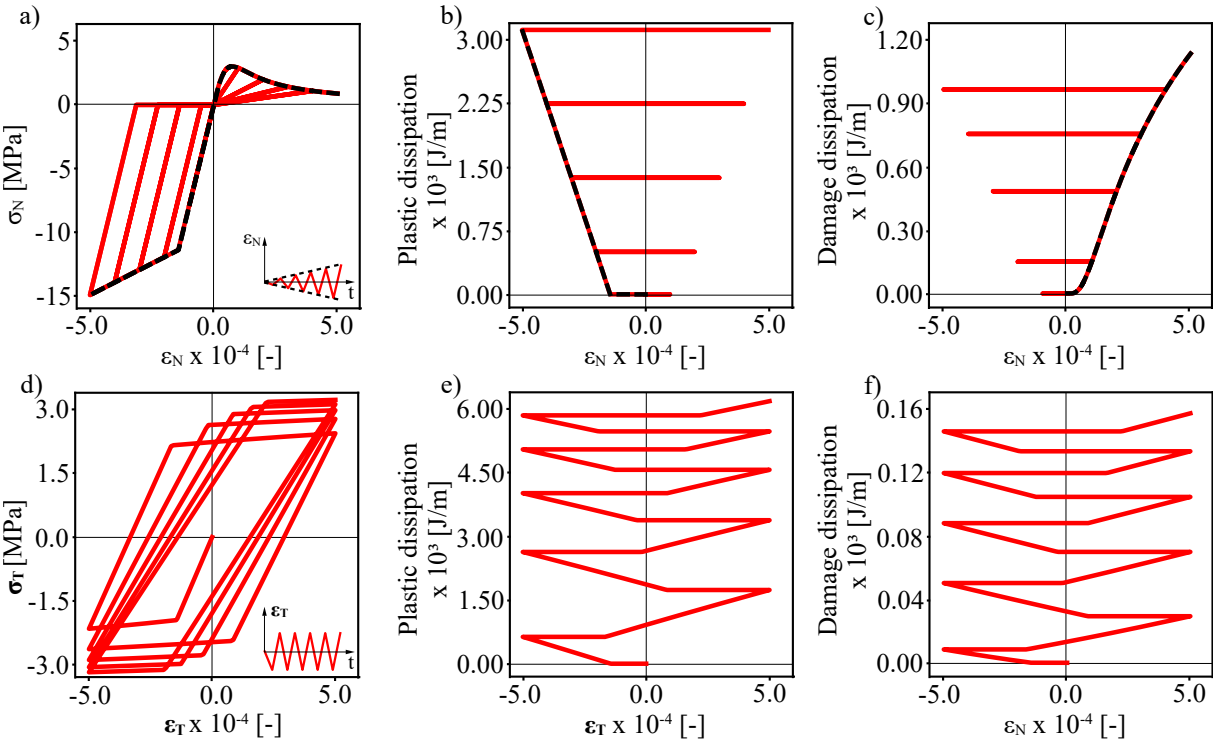

Figure 3: Elementary interface behaviour, above normal direction, below tangential direction, a) and d) stress-strain curve, b) and e) plastic dissipation, c) and f) damage dissipation

stiffness. The coupling of damage and plasticity leading to this gradual stiffness reduction is documented in Figs. 3ef, revealing that damage evolves upon reaching the tangential threshold with an increasing plastic slip.

The macroscopic energy dissipation is evaluated by integrating the contributions of each microplane for the normal and tangential directions:

$$\mathcal{D}_{\text{int}}^{\text{mac}} = \frac{3}{2\pi}\int_{\Omega}\mathcal{D}_{\text{int}}^{\text{mic}}d\Omega = \frac{3}{2\pi}\int_{\Omega}\mathcal{D}_{\text{int}}^{\text{N}}d\Omega + \frac{3}{2\pi}\int_{\Omega}\mathcal{D}_{\text{int}}^{\text{T}}d\Omega. \tag{14}$$

3.3 Evaluation of energy dissipated in cyclic compressive tests

The described approach has been used to evaluate the energy dissipation in cylindrical concrete specimens exposed to a compressive step-wise cyclic loading scenario. The concrete grade used in the test series described in [11] was C80 with an average compressive strength f_{c} of 101.38 MPa. The loading scenario consisted of a step-wise increasing loading, starting at 50% of the maximum compressive strength, and increasing by 5% every 10 cycles. The minimum loading was kept constant at 10 % of f_{c}. The measured stress-strain response for three selected tests is depicted in Fig. 4a. The dissipation within each hysteretic loop has been evaluated for the loading history by identifying the intersection point of the descending and ascending branches in each load cycle and numerical integration within the enclosed area. The resulting curve is shown in Fig. 4b. The energy dissipation accumulated during the whole history within the loops is plotted in Fig. 4c.

To gain a deeper insight into the way that energy is being dissipated under cyclic compression, the microplane material model MS1 has been employed. The objective is to have a qualitative comparison between the energy dissipated within and outside the hysteretic loops. The simulated stress-strain response of the material is depicted in Fig. 4d. In Fig. 4e the energy dissipated within hysteretic loops and the complete dissipation in each cycle are compared.

It is obvious that the increase of the upper load level leads to a rapid energy dissipation due to damage and friction which is represented by the peaks in Fig. 4e. At the same time, the amount of total energy dissipated during the uniform load cycles within each load level is significantly larger than the area of the hysteretic loop represented by the green curve. The cumulative evolution of the energy dissipation ascribed to the loops and the total energy dissipation is depicted in Fig. 4f.

The resolved evaluation of the energy dissipation using the model can now be compared with the curve shown in Fig. 4b obtained from the hysteretic loop evaluation of the experimental response. This curve qualitatively corresponds to the green curve in Fig. 4e. Even though the two curves do not correspond quantitatively, the study documents that the true energy dissipated in the experiment is significantly larger than the area of the hysteretic loops. Accurate evaluation requires a refined model calibration, which can reflect a wider shape of the hysteretic loops. The improvements of the model are currently being elaborated.

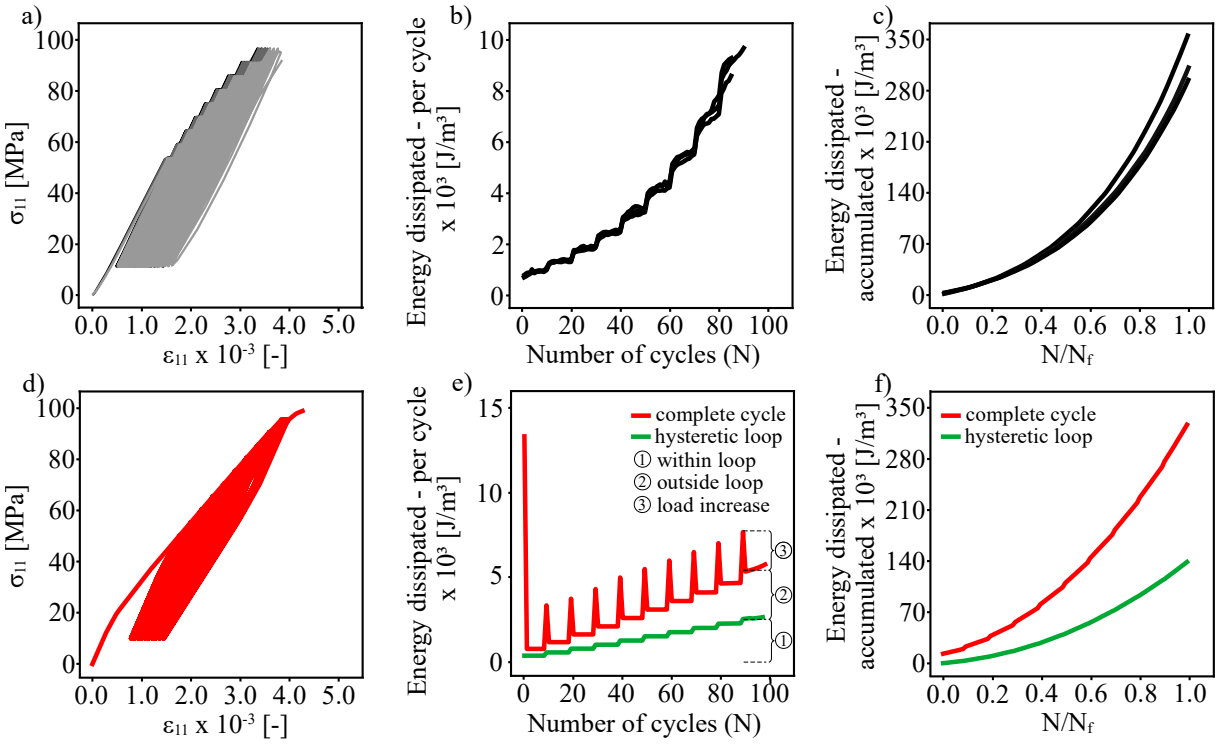

Figure 4: Above experimental data, below numeral results, a) and d) stress-strain curve, b) and e) energy dissipated within a cycle, c) and f) accumulated dissipated energy

3.4 Analysis of dissipative mechanisms governing the fatigue response

Once the importance of the dissipation evaluation method accounting for the complete cycle has been highlighted, numerical studies quantifying the energy dissipated for uniform fatigue compressive loading can be addressed. Several authors have reported that the total amount of energy being dissipated during a cyclic or fatigue test depends on the applied loading scenario [8, 9]. For constant loading scenarios, experimental results reveal that uniform fatigue loading with lower maximum load levels lead to a longer fatigue life and, thus, to a larger accumulated energy dissipation. This trend is well captured by the microplane material model MS1. Energy dissipation corresponding to three varied load levels is evaluated for the concrete C80 with material parameters presented in [4], The obtained results are summarized in Table 1 and Fig. 5. It worth noting, that for lower maximum load levels, there is a significant increase of the energy dissipated by frictional slip, as documented in Fig. 5b. On the other hand, the amount of energy dissipated due to damage is much less sensitive to the applied level of maximum fatigue load.

4 SEQUENCE EFFECT INVESTIGATION

In reality, structures undergo cyclic loading with varying amplitudes in various sequences during their service life [12]. The Fib Model Code for Concrete Structures 2010 [1] proposes to apply the Palmgren-Miner (P-M) rule to account for non-uniform fatigue load-

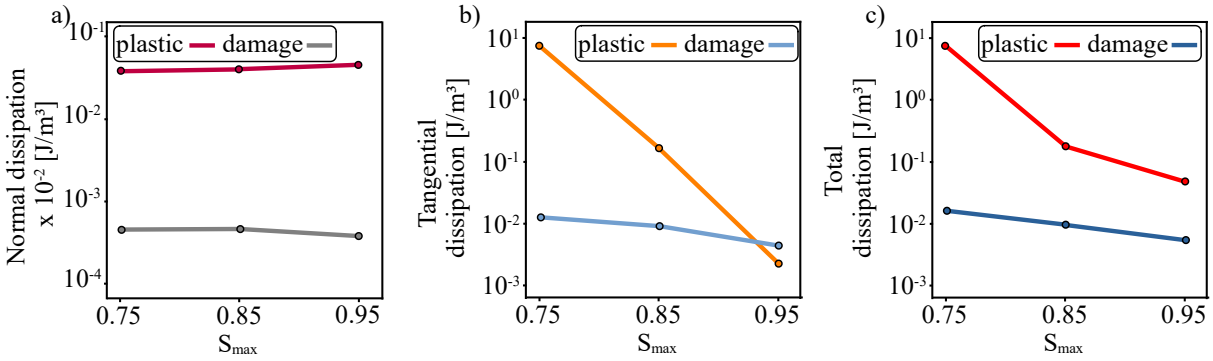

Figure 5: a) plastic and damage energy dissipation in normal direction, b) plastic and damage energy dissipation in tangential direction, c) total plastic and damage dissipation.

Table 1: Evaluation of the energy dissipation components for three different constant load levels

$S_{\max}$	Cycles	Plastic normal $[J/m^3]$	Plastic tan. $[J/m^3]$	Total plastic $[J/m^3]$	Damage normal $[J/m^3]$	Damage tan. $[J/m^3]$	Total damage $[J/m^3]$	Total dissipation $[J/m^3]$
0.95	21	4.48e-2	2.28e-3	4.71e-2	4.28e-4	4.87e-3	5.30e-3	5.24e-2
		85.50%	4.38%	89.88%	0.82 %	9.29%	10.12%	
0.85	1357	4.00e-2	1.19e-1	1.59e-1	4.64e-4	8.97e-3	9.44e-3	1.68e-1
		23.75%	70.65%	94.40%	0.27 %	5.32%	5.60%	
0.75	126913	3.77e-2	7.54e0	7.57	4.61e-4	1.26e-2	1.31e-2	7.59
		0.50%	99.32%	99.82%	0.01 %	0.17%	0.18%	

ing. This rule assumes a linear accumulation of fatigue damage, so that the fatigue life under a loading scenario consisting of several load ranges with variable amplitudes can be estimated as a linear interpolation of the fatigue lives corresponding to each of the individual load ranges. It must be pointed out that there is no experimental evidence that supports this rule. Moreover, the available experimental data suggests that the P-M rule can deliver unsafe fatigue life predictions [11, 13]. Therefore, the effects on the fatigue life in response to compressive loading with variable amplitudes must be studied in more detail.

The detailed knowledge of the dissipative mechanisms governing the fatigue propagation characterized in terms of their energy dissipation represents an attractive option which would allow a prediction of the fatigue life based on the energetic considerations. Such aims have been reported e.g. by [14] hypothesizing that the amount of energy dissipated or absorbed by concrete for monotonic and fatigue loading remains constant. However,as stated in [15] the size of the fracture process zone is different for the monotonic and fatigue loading process. Reflection of this phenomenon and the evaluations of the damage induced energy dissipation are the prerequisites for an improved prediction

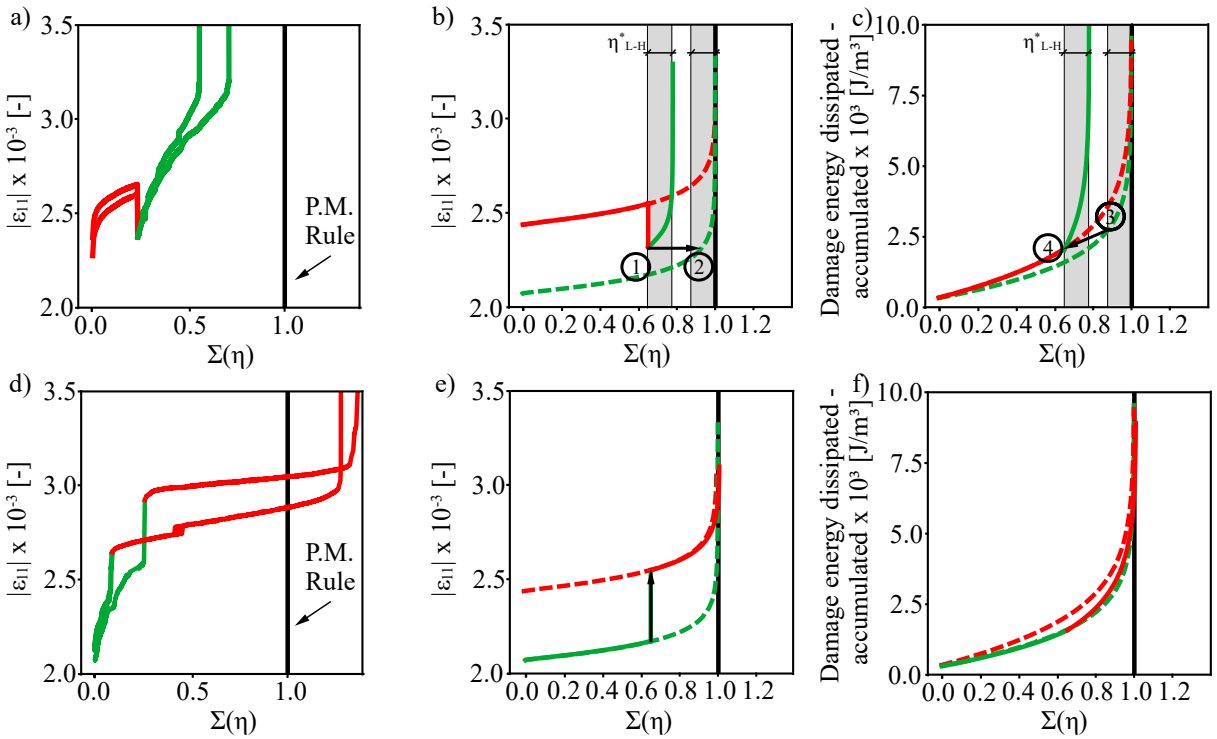

Figure 6: Order effect investigation. Above H-L loading scenario, below L-H loading scenario for concrete C80 presented at [11] fatigue creep curves compared with simulated fatigue creep curves, a) H-L experimental fatigue creep curve, b) H-L numerical fatigue creep curve, c) numerical H-L damage energy dissipation, d) L-H experimental fatigue creep curve, e) L-H numerical fatigue creep curve, f) numerical L-H damage energy dissipation

methods of fatigue life in response to fatigue loading with variable amplitudes. Then, a superposition of the damage induced energy dissipation profiles for constant fatigue loading, as exposed in [11] for a non-uniform loading scenario appears justified.

To demonstrate this hypothesis, the sequence effect of two loading ranges denoted as H and L with upper load levels $S_{\max} = 0.85$ and $S_{\max} = 0.75$, respectively, is studied Fig 6. The lower load level was set to $S_{\min} = 0.2$ for both ranges. With the cycles-to-failure for each loading range applied individually denoted as $N_{\mathrm{H}}^{\mathrm{f}}$ and $N_{\mathrm{L}}^{\mathrm{f}}$, the P-M rule states that if the H loading range was applied first until 65% of its fatigue life, i.e. $0.65N_{\mathrm{H}}^{\mathrm{f}}$, the material will resist 35% of its fatigue life, i.e. $0.35N_{\mathrm{L}}^{\mathrm{f}}$, after switching to the L load level.

The two corresponding scenarios, H-L and two L-H are studied using numerical simulations with the microplane model MS1 in Figs. 6be with the material parameters set as specified in [4]. The lifetime on the horizontal axis is normalized with respect to the lifetime prediction by the P-M rule. The experimental response for the H-L and L-H scenarios obtained in [11] for the concrete grade C80 is is provided in Figs. 6ad for qualitative comparison. Both the simulations and experimental data show that for the H-L scenario a failure occurs considerably earlier than predicted by the P-M rule. For the L-H scenario, both experimental and numerical results deliver an extension of the fatigue

life with respect to the H-L loading scenario.

Fig. 6b can be used to explain the existence of the sequence effect. Regarding the H-L scenario depicted as the red curve in Fig. 6b, let us hypothesize that the state of the material corresponding to the strain attained after the switch to the lower level marked as point (1), is equal to the state of the material attained for the the L loading scenario with same strain denoted as point (2). Then the residual life of the H-L scenario can be estimated by shifting the green curve from point (2) to the point (1). This shift explains why the H-L scenario must lead to a reduced fatigue life compared to the P-M rule.

The profile of damage induced energy dissipation is included in Figs. 6c. It can be used to illustrate the hypothesis formulated in [11] which states that under the assumption of uniform energy dissipation within the volume of a tested specimen, residual fatigue lives can be superposed by shifting between energy dissipation profiles obtained for uniform loading ranges at L and H levels. The obtained curves are used to indicate the possibility to numerically identify points (3) and (4) with the same residual fatigue life in the load scenarios H-L and L. The availability of a model that can resolve the individual dissipative mechanisms provides a chance to further refine the superposition rules based on energetic arguments as a basis for more realistic predictions of the sequence effect.

5 CONCLUSIONS

Experimental observations indicate that the well-established method for measuring the energy dissipated by concrete during fatigue loading, evaluating the area contained in hysteretic loops, can not properly reflect the total amount of energy dissipation. The new microplane material model MS1 was employed to evaluate the individual components of the dissipated energy for three different loading ranges. They reveal that for high-cycle fatigue the dominating amount of energy dissipation is due to cumulative plastic sliding. On the other hand, for low-cycle fatigue, the damage induced dissipation reaches a comparable range. Numerical studies evaluating the sequence effect deliver a reduced fatigue life for H-L case, matching the trend observed in the available experimental data.

ACKNOWLEDGMENT

The work was supported by the German Research Foundation (DFG) in the scope of the Priority Program SPP2020 “Cyclic deterioration of high-performance concrete in an experimental virtual lab.” (Project number: 441550460). This support is gratefully acknowledged.

REFERENCES

[1] *Fib model code for concrete structures 2010*. Document Competence Center Siegmar Kästl eK, Germany, (2010).

[2] Su, Eric CM and Hsu, Thomas TC. Biaxial Compression Datigue and the Discontinuity of Concrete. *Materials Journal* (1988) **85**:178–188.

[3] Zhang, B and Phillips, DV and Wu, K. Further research on fatigue properties of plain concrete. *Magazine of concrete research* (1997) **49**:241–252.

[4] Baktheer, A., Aguilar, M. and Chudoba, R. Microplane fatigue model MS1 for plain concrete under compression with damage evolution driven by cumulative inelastic shear strain. *International Journal of Plasticity* (2021)

[5] Skarzynski, L. ,Marzec, I. and Tejchman, J. Fracture evolution in concrete compressive fatigue experiments based on X-ray micro-CT images. *International Journal of Fatigue* (2019) **122**:241–252.

[6] Baktheer, A. and Chudoba, R. Pressure-sensitive bond fatigue model with damage evolution driven by cumulative slip: Thermodynamic formulation and applications to steel- and FRP-concrete bond. *International Journal of Fatigue* (2018) **113**:277 - 289.

[7] Do, M. T., Chaallal, O. and Aïtcin, P. C. Fatigue behavior of high-performance concrete. *Journal of Materials in civil Engineering* (1993) **5**:96–111.

[8] Song, Z., Frühwirt, T., & Konietzky, H. Characteristics of dissipated energy of concrete subjected to cyclic loading. *Construction and Building Materials* (2018) **168**:47–60.

[9] Bode, M. and Marx, S. Energetic damage analysis regarding the fatigue of concrete. *Structural Concrete* (2021) **22**:E851–E859.

[10] Baktheer, A. , Spartali, H, Hegger, J. and Chudoba, R. High-cycle fatigue of bond in reinforced high-strength concrete under push-in loading characterized using the modified beam-end test. *Cement and Concrete Composites* (2021) **118**:103978.

[11] Baktheer, A. and Chudoba, R. Experimental and theoretical evidence for the load sequence effect in the compressive fatigue behavior of concrete. *Materials and Structures* (2021) **54**:1–23.

[12] El Aghoury, I., and Galal, K. A fatigue stress-life damage accumulation model for variable amplitude fatigue loading based on virtual target life. *Engineering structures* (2013) **52**:621–628.

[13] Holmen, J. O. Fatigue of concrete by constant and variable amplitude loading. *Special Publication* (1982) **75**:71–110.

[14] Tepfers, R., Hedberg, B., and Szczekocki, G. Absorption of energy in fatigue loading of plain concrete. *Matériaux et Construction* (1984) **17**:59–64.

[15] Bandelt, M. J., Frank T. E., Lepech M. D and and Billington S. L. Bond behavior and interface modeling of reinforced high-performance fiber-reinforced cementitious composites. *Cement and Concrete Composites* (2017) **83**:188-201.